An Evaluation of Ultra Wideband Technology for Indoor Ranging

Camillo Gentile and Alfred Kik
National Institute of Standards and Technology
Wireless Communication Technologies Group
Gaithersburg, Maryland, USA
{camillo.gentile, alfred.elkik}@nist.gov

***Abstract*— Ultra wideband technology shows promise for precision ranging due to its fine time resolution to resolve multipath fading and the presence of lower frequencies in the baseband to penetrate walls. While a concerted effort has been conducted in the extensive modeling of the indoor UWB channel in recent years, to our knowledge only two papers have reported ranging performance, but for limited range and fixed bandwidth and center frequency. In principle boosting power can guarantee connectivity between transmitter and receiver, but not precision due to the distorting effects of walls and other objects in the direct path. In order to gauge the limits of UWB ranging, we carry out 5000 measurements up to an unprecedented 45 m in non line-of-sight conditions in four separate buildings with dominant wall material varying from sheet rock to steel. In addition, we report performance for varying bandwidth and center frequency of the system.**

***Index Terms*— Channel modeling, frequency domain, vector network analyzer**

I. Introduction

Ultra wideband (UWB) signals are characterized by a bandwidth greater than 500 MHz or one exceeding 20% of the center frequency of radiation [1], [2]. Such technology shows promise for indoor ranging due to its fine time resolution to resolve multipath fading and the presence of lower frequencies in the baseband to penetrate walls. The approval of the FCC unlicensed band from 3.1-10.6 GHz in 2002 has prompted a concerted effort in the extensive modeling of the indoor UWB channel in recent years. Irahhauten provides a comprehensive overview of indoor UWB measurements in the time and frequency domains [3]. Table I summarizes this overview, but augmented to include reported measurements to date. Most references in the table provide channel models characterized by path loss, small-scale fading, and delay spread. The most comprehensive of the models proposed by Molisch also includes frequency fading and clusters in the multipath profile. The latter gathers measurements conducted by separate parties with similar parameters to investigate not only three indoor environments, but also two outdoor environments and the body area network.

Emergency response systems in particular require that mobile rescue devices inside a building maintain connectivity to at least three base stations deployed outside to estimate their locations through triangulation of ranges [12]. In principle boosting transmission power to levels above the FCC mask can ensure such connectivity for large buildings, however connectivity alone cannot guarantee precision due to the distorting effects of walls (and other objects) in the direct path. The number of wall interactions in general increases with range, leading to a degradation in performance due to the physical limits of the system. This evaluation quantifies the degradation up to an unprecedented 45 m due to the large dynamic range of our measurement system.

	Prin. Investigator	f range	environment	range
time	Yano [4]	1.25-2.75 GHz	office	17 m
	Cassioli [2], [6], [7]	3.6-6 GHz	office	18 m
	Prettie [5]	2-8 GHz	res.	20 m
frequency	Kunisch [8]	1-11 GHz	office	10 m
	Keignart [9]	2-6 GHz	office / res.	20 m
	Ghassemzadeh [10]	2-8 GHz	res. / commercial	15 m
	Molisch [11]	3-10 GHz	res. / industrial / office	28 m 20 m

TABLE I
Overview of reported indoor UWB measurements.

Similar to [8], [9], [10], [11], we carry out 5000 measurements in the frequency domain from 2-8 GHz, however in a homogeneous fashion throughout four separate buildings. Rather than extract a channel model, we report the ranging performance based on time-of-flight estimation. To our knowledge, only Denis and Scholtz have performed such a study [13], [14], [15], however to date no effort has been dedicated to the evaluation of this performance according to variation in system parameters. Specifically, the main contribution of this paper is a study of the relationship between range error and:

- *bandwidth*: precision increases with bandwidth, but carries diminishing returns with the additional expense;
- *center frequency*: lower frequencies penetrate materials better[1];
- *construction material*: compare performance with typical building construction materials varying as sheet rock (easy), plaster, cinder block, to steel (most difficult) to gauge lower and upper bounds on the technology, rather than with building layout (i.e. office, residential typically have the same wall materials);
- *long range*: the high dynamic range of our system allows us to span 45 m and examine the limits in the technology inherent to the interaction with up to 12 walls.

We also compute path loss for all the experiments to render

[1]Cassioli [16] performed a similar study of the relationship between path loss and center frequency.

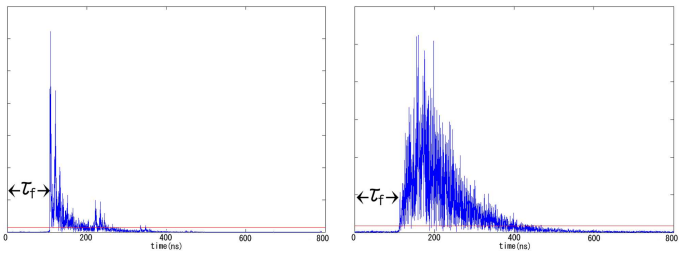

(a) LOS (b) NLOS

Fig. 1. The impulse response of the channel.

the results independent of our particular transmitter power and receiver sensitivity.

The paper reads as follows: Section II describes the technique for channel measurement in the frequency domain used to estimate range, and Section III provides the details of our equipment setup. Section IV outlines our suite of measurements and presents the results both through statistical measures and in graphical format, followed by conclusions in the last section.

II. Preliminaries

A. The indoor propagation channel

The indoor propagation channel is conventionally modeled by an impulse train corresponding to K multipath arrivals indexed through k [17]:

$$h(t) = \sum_{k=0}^{K-1} \alpha_k \delta(t - \tau_k), \tag{1}$$

where τ_k represents the delay of the arrival in propagating between the transmitter and the receiver, and α_k represents the complex-valued amplitude which accounts for both attenuation and phase change due to reflection, diffraction, and other specular effects introduced by walls on its path. Fig. 1(a) displays a typical impulse response for *line-of-sight* (LOS) conditions between the transmitter and the receiver. Ranging systems based on *time-of-flight* estimate the delay τ_f corresponding to the arrival of the first impulse in the response, or *leading edge*. Since the signal propagates at the speed of light c in free space, the range between the radios is estimated as $c \cdot \tau_f$.

Indoor propagation delivers many and closely-packed arrivals to the receiver inherent to the smaller dimensions of objects compared to outdoors. Ultra wideband technology transmits pulses sufficiently narrow in time to allow for path resolution at the receiver, avoiding overlap of the pulses which may otherwise combine in a destructive manner and render poor results. Even though UWB can successfully isolate multipath arrivals, the interaction of the signals with the walls and other objects distorts the signal. In *non line-of-sight* (NLOS) conditions such as in Fig. 1(b), the leading-edge path propagating through walls may appear attenuated with respect to another reflected path, or even buried below the noise floor of the channel. Even if detectable, the leading edge propagates through walls at a slower speed than light, adding an irrecoverable delay with each in the estimation of τ_f since the number of walls and construction material are unknown a priori: sheet rock (cinder block) introduces an additional delay of 1.8 $\frac{\text{ns}}{\text{m wall}}$ (3.4 $\frac{\text{ns}}{\text{m wall}}$) for a total error of 54 cm (102 cm) through 10 walls typically 10 cm thick [18]. This phenomenon places a physical limit on the performance of the system.

B. Time-of-flight estimation

The impulse response of the channel in (1) has the corresponding frequency response

$$H(f) = \sum_{k=0}^{K-1} \alpha_k e^{-j2\pi f \tau_k}, \tag{2}$$

suggesting that the channel can be characterized through frequency measurements. A vector network analyzer (VNA) can measure $H(f)$ at discrete values of f with sampling interval Δf; a discrete frequency spectrum translates to a periodic signal in the time domain with period $\frac{1}{\Delta f}$ [19]. Choosing Δf = 1.25 MHz allows for a maximum multipath spread of 800 ns, which proves sufficient throughout all four buildings for the arrivals to subside and avoid time aliasing. The following section provides the details of our measurement system.

Characterizing the channel in the frequency domain offers an important advantage over transmitting a fixed pulse and recording the impulse response directly: namely once we sweep the 2-8 GHz band of interest, a sub-band with bandwidth B and the center frequency f_c can be selected a posteriori in varying the parameters of the system. The corresponding impulse response can be recovered through the Inverse Discrete Fourier Transform (IDFT) [20]:

$$h(t) = \frac{1}{2} \sum_{l=0}^{\frac{B}{\Delta f}} H(f) e^{j2\pi f t} + H^*(f) e^{-j2\pi f t}, \tag{3}$$

where $f = f_c - \frac{B}{2} + l \cdot \Delta f$.

In order to estimate τ_f, we first apply a Gaussian window to the sub-band; this reduce the sidelobes in the time domain after taking the IDFT. A simple but effective thresholding technique estimates the leading edge from the impulse response: it calculates the mean μ and standard deviation σ of a fixed-length sliding window originating at the beginning of the impulse response. The length of the window is $20 \cdot \frac{1}{B}$ ns, and so 3.33 ns for 6 GHz. We select the leading edge as the first value in front of the window, occurring at time τ_f, to exceed a dynamic threshold. Assuming a Gaussian distribution for the values of the noise before the leading-edge [21], the dynamic threshold is defined as $\mu + a \cdot \sigma$, where the factor $a \in (12, 20)$ was optimized for each bandwidth. The thresholder corresponded exactly to our visual perception of the leading-edge in greater than 98% of the trials, and in the remaining percentage deviated by only few nanoseconds. Other papers

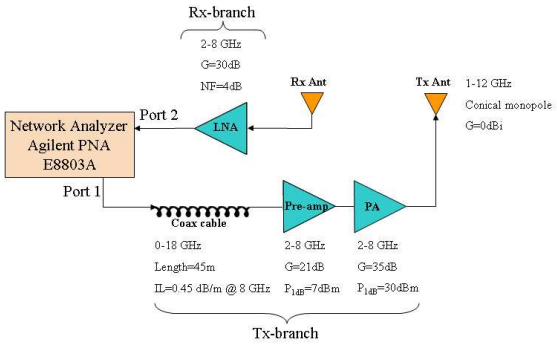

Fig. 2. The measurement system using the Vector Network Analyzer.

in literature propose alternative thresholds for estimating τ_f in UWB ranging systems tailored to their specific measurements [15], [21], [22].

III. Measurement System

The diagram of our measurement system appears in Fig. 2. As explained in the previous section, the VNA emits a series of tones with frequency f at Port 1 and measures the relative amplitude and phase $S_{21}(f)$ at Port 2, providing automatic phase synchronization between the two ports. The long cable enables variable positioning of the omnidirectional conical monopole antennas from each other throughout the test area. The pre-amplifier and power amplifier on the transmit branch boost the signal such that it radiates at approximately 30 dBm from the antenna. After it passes through the channel, the low-noise amplifier (LNA) on the receiver branch boosts the signal above the noise floor of Port 2 before feeding it back.

Full two-port calibration of the VNA precedes measuring the $S_{21}(f)$-parameter of the network in Fig. 2 expressed through

$$S_{21}(f) = H_{Tx}^{bra}(f) \cdot H_{Tx}^{ant}(f) \cdot H(f) \cdot H_{Rx}^{ant}(f) \cdot H_{Rx}^{bra}(f), \quad (4)$$

the product composed from the Tx-branch, the Tx-antenna, the propagation channel, the Rx-antenna, and the Rx-branch. The frequency response of the channel H is extracted by individually measuring in advance the transmission responses $H_{Tx}^{bra}, H_{Rx}^{bra}$, and $H^{ant} = H_{Tx}^{ant} = H_{Rx}^{ant}$ (assuming identical antennas) and de-embedding them from (4). The characteristics of the antennas were measured by separating them by a distance of 1.5 m to avoid the near-field effects and spatially averaging them through rotation with respect to each other every ten degrees. Their height was set to 1.7 m (average human height).

Note in particular the following implementation considerations:

- to account for the frequency-dependent loss in the long cable when operating across such a large bandwidth, we ramped up the emitted power at Port 1 with increasing frequency to radiate from the antenna at approximately 30 dBm across the whole band;
- we removed the LNA from the network in experiments with range below 10 m to protect it from overload and also avert its operation in the non-linear region;
- to extend the dynamic range of our system, we exploited the configurable test set option of the VNA to reverse the signal path in the coupler of Port 2 and bypass the 12 dB loss associated with the coupler arm. The dynamic range of the propagation channel corresponds to 144 dB as computed through [9] for an IF bandwidth of 1 kHz and a SNR of 10 dB at the receiver;
- to account for small-scale fading in estimating path loss (and also for temporal variation in the measurements), for each experiment we centered a 5×5 grid constructed from a wooden plank on the floor about the nominal location of the receiver antenna. The distance between the grid points was 15 cm, corresponding to a full wavelength at 2 GHz, ensuring spatial independence between the measured points for a total of 25 sub-experiments.

building	wall material	LOS range (10)	NLOS range (40)
NIST North	sheet rock / aluminum studs	1.2-24.3 m	1.7-40.7 m max wall#: 12
Child Care	plaster / wooden studs	2.0-15.7 m	4.7-33.0 m max wall#: 7
Sound	cinder block	3.4-45.0 m	5.9-40.8 m max wall#: 9
Plant	steel	2.9-43.7 m	4.9-44.0 m max wall#: 8

TABLE II
EXPERIMENTS CONDUCTED IN MEASUREMENT CAMPAIGN.

IV. Experimental Setup and Results

A. Experimental Setup

The measurement campaign was conducted in four separate buildings on the NIST campus in Gaithersburg, Maryland, each constructed from a dominant wall material varying from sheet rock (easy) to steel (most difficult). This variety allows gauging lower and upper bounds on the performance of UWB technology for indoor ranging. Table II summarizes the 50 experiments in each building (10 LOS and 40 NLOS), including the maximum number of walls separating the transmitter and receiver. As an example, consider the map of *NIST North* in Fig. 3: the experiments were drawn from the two sets of 31 transmitter locations and 5 receiver locations, indicated by the solid and empty circles respectively, to the end of achieving a uniform distribution in range in both LOS and NLOS conditions. The solid line identifies the experiment with the longest range and the 12 walls between the transmitter and receiver. For the most part, the measurements were taken after hours to minimize any disturbance due to the movement of personnel throughout the buildings.

B. Results

This subsection reports the range error of each sub-experiment defined as the absolute difference between the estimated range and the ground-truth range at the corresponding

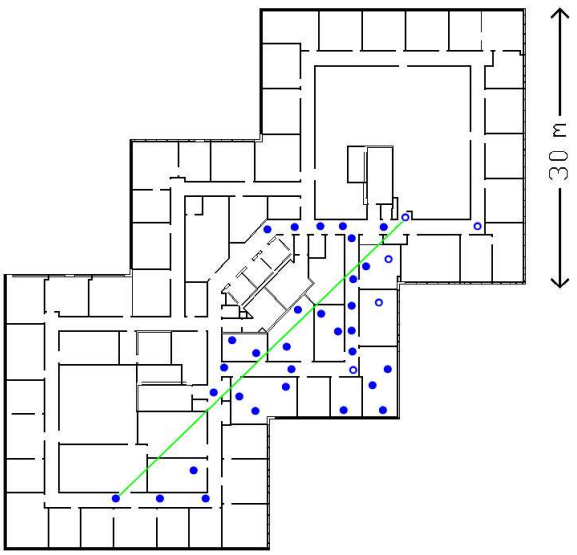

Fig. 3. The map of the *NIST North* building.

point on the grid. The ground-truth ranges were computed by pinpointing the nominal locations of the transmitter and receiver with a laser tape for each experiment in the campaign, and automatically extrapolating the 25 ranges on the grid using a CAD model of each building layout, for a total of 5000 measurements (50 experiments × 25 sub-experiments × 4 buildings). Table III reports the statistics of the ensemble of sub-experiments corresponding to each cross-labeled scenario in the following format: $\frac{\mu_e(\text{cm}),\ \sigma_e(\text{cm})}{\min_e(\text{cm}),\ \max_e(\text{cm})}$, $\frac{PL_0(\text{dB}),\ \gamma}{}$, where $\mu_e, \sigma_e, \min_e$ and $\max_e$ are the mean, standard deviation, minimum, and maximum values of the range error, and PL_0 and γ respectively characterize the reference loss at d_0 = 1 m and the exponent of the single-slope path loss model [10]:

$$PL(d)\ (\text{dB}) = PL_0 + 10\gamma \log_{10}\left(\frac{d}{d_0}\right). \qquad (5)$$

Reporting the path loss for each scenario disassociates the results from our particular transmitter power and receiver sensitivity.

The plots in Fig. 4 illustrate the range error (cm) versus the ground-truth range (m) for selected scenarios in the table[2]. The mean μ_e of each scenario from Table III also appears on the plot as a dark square to highlight the trend in parameter variation. Fig. 4(a) display the results for the LOS experiments in *Sound* with f_c = 5 GHz while varying B = {0.5, 1, 2, 4, 6} GHz, the latter multiplexed on the abscissa. The error lies within 12 cm (22 cm) for 6 GHz (4 GHz) up to 45 m. No obvious correlation exists between error and range, however performance improves significantly with increasing bandwidth, but at diminishing returns: μ_e drops from 49 to 34 cm from 0.5 to 1 GHz, but only from 9 to 6 cm from 4 to 6 GHz; this phenomenon holds true throughout all scenarios. The LOS experiments in the other three buildings exhibit similar behavior as in *Sound*, with the best results in *NIST North*. Overall the system delivers μ_e = 5 cm for 6 GHz throughout all four buildings tested.

Figs. 4(b-e) display the NLOS experiments in all four buildings with f_c = 5 GHz while varying B = {0.5, 1, 2, 4, 6} GHz. While notably worse than the LOS experiments, the error still lies within 40 cm (1% relative error) in *NIST North* for a bandwidth greater than 4 GHz (except for three of the 40 experiments) and yields μ_e = 23 cm at 6 GHz; these exceptions however attest to the breakdown of the technology at longer ranges experienced throughout all buildings. The mean μ_e increases to 29 and 80 cm for 6 GHz in *Child Care* and *Sound* with most of the errors below 100 (3%) and 150 cm (4%) respectively; considering that the signal traverses up to 40m and 9 walls in these two buildings, the results fare quite well, especially since computing location by triangulating three or more ranges can reduce the location error by an order of magnitude with respect to the range error [12]. Despite the small path loss in *Plant* due to the favorable properties of the walls which behave as waveguides, the system provides μ_e = 386 cm and an error less than 350 cm only up to 15 m at 6 GHz, clearly manifesting the impenetrable properties of metal by the direct path. Note that the maximum path loss of 125 dB across all experiments occurs in *Sound*, and still lies well within the dynamic range of our system.

In most scenarios across the four buildings, the error increases substantially at higher center frequencies due to larger associated path losses as quantified in Table III; this phenomenon surfaces more in *Sound* due to thicker walls than in *NIST North* and *Child Care*. Figs. 4(f-h) display the NLOS experiments in the *Sound* building for B = 1, 2, and 4 GHz while varying f_c, the latter multiplexed on the abscissa. For all three bandwidths, μ_e increases about 30 cm from the lowest to the highest center frequency.

V. Conclusions and Further Work

Our nominal ranging system with 6 GHz bandwidth and 5 GHz center frequency delivers a mean range error of 5 cm in LOS conditions up to 45 m throughout all four buildings tested. This error increases to 23, 29, and 80 cm for sheet rock, plaster, and cinder block wall materials respectively in NLOS conditions; the system ranges within 350 cm up to 15 m in the steel building, but the performance degrades rapidly thereafter. The ranging precision improves significantly when raising the bandwidth from 0.5 GHz to 4 GHz, but at a diminishing rate, and shows virtually no further improvement at 6 GHz. The error increases about 30 cm from a center frequency of 3 to 7 GHz due to larger path loss of the latter.

[2]To avoid clutter, each point indicates the range error averaged over the 25 sub-experiments versus the nominal range of the experiment.

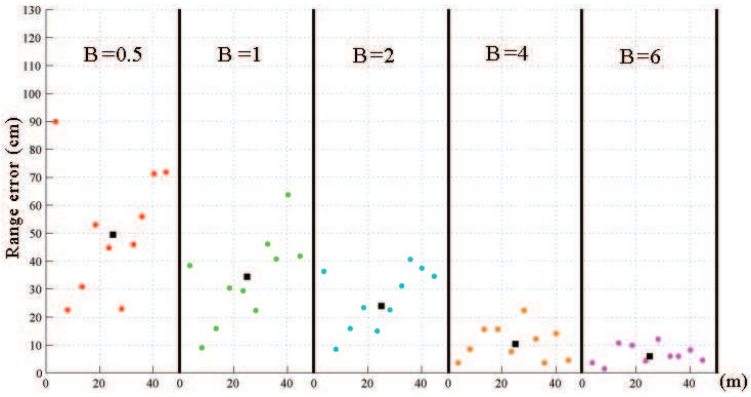

(a) *Sound*, LOS, f_c = 5 GHz

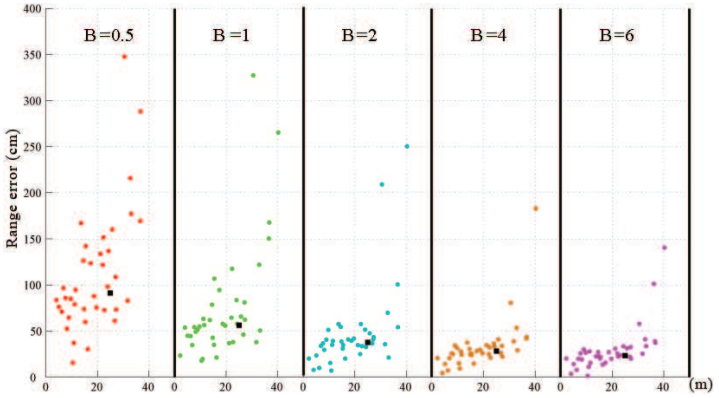

(b) *NIST North*, NLOS, f_c = 5 GHz

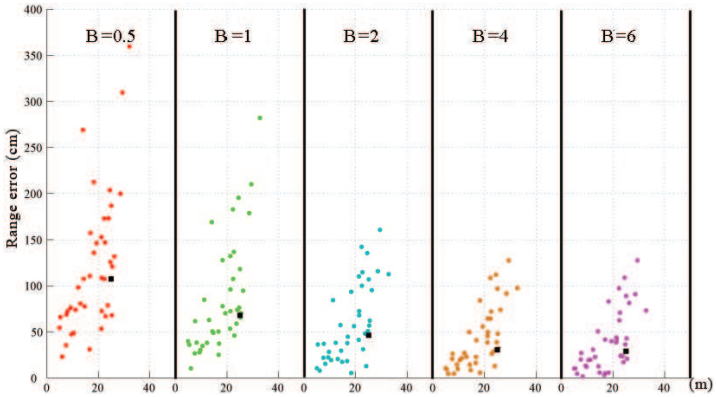

(c) *Child Care*, NLOS, f_c = 5 GHz

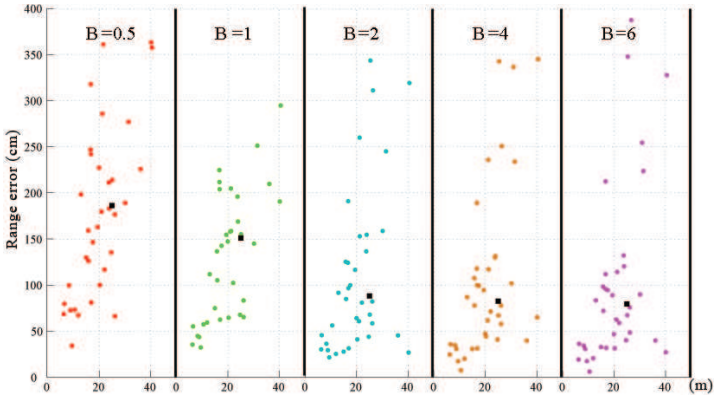

(d) *Sound*, NLOS, f_c = 5 GHz

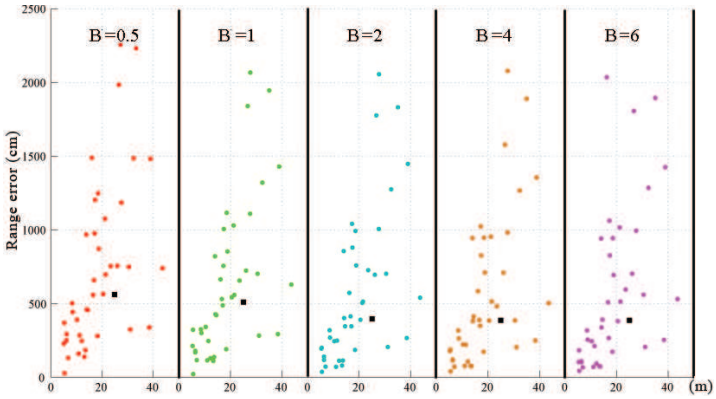

(e) *Plant*, NLOS, f_c = 5 GHz

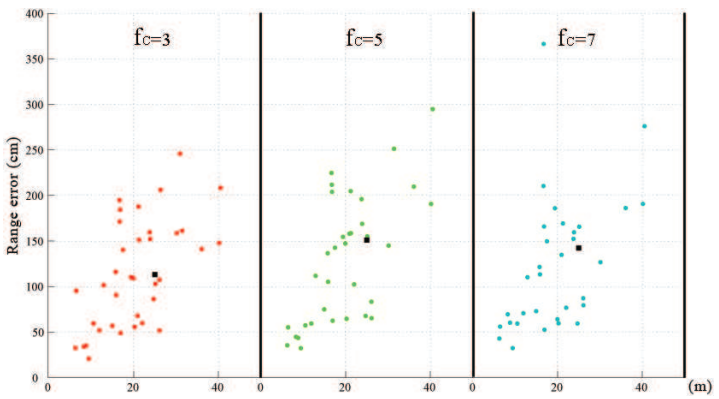

(f) *Sound*, NLOS, B = 1 GHz

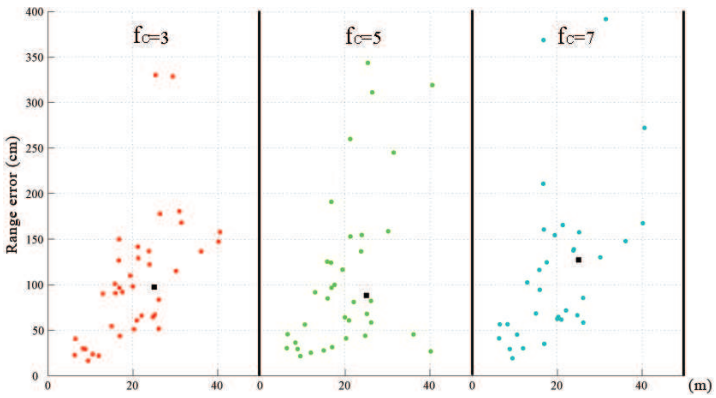

(g) *Sound*, NLOS, B = 2 GHz

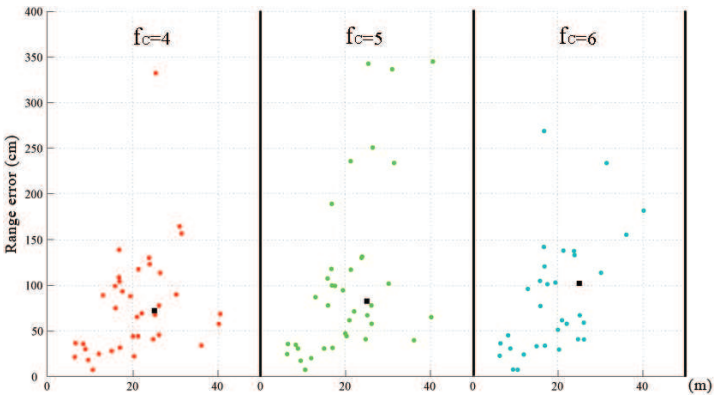

(h) *Sound*, NLOS, B = 4 GHz

Fig. 4. Range error (cm) versus ground-truth range (m) for selected scenarios.

	building	B = 0.5	B = 1			B = 2			B = 4			B = 6
		f_c = 5	f_c = 3	f_c = 5	f_c = 7	f_c = 3	f_c = 5	f_c = 7	f_c = 4	f_c = 5	f_c = 6	f_c = 5
LOS	*NIST*	34, 13	16, 7	17, 7	21, 13	3, 6	12, 7	18, 9	3, 4	6, 4	6, 3	3, 4
	North	17, 56	6, 37	6, 33	8, 47	1, 20	3, 21	2, 31	1, 12	1, 12	3, 12	1, 13
		42, 1.6	42, 1.3	42, 1.5	42, 1.6	40, 1.4	43, 1.5	43, 1.6	41, 1.4	44, 1.3	43, 1.5	42, 1.4
	Child	23, 30	11, 7	11, 6	10, 10	9, 4	9, 5	9, 5	6, 15	6, 58	10, 7	4, 6
	Care	9, 103	7, 26	8, 24	6, 35	4, 20	4, 22	4, 20	2, 50	2, 18	1, 18	0, 15
		43, 2.2	40, 2.2	44, 2.1	44, 2.1	38, 2.3	45, 1.8	46, 2.0	41, 2.1	45, 1.8	45, 1.9	42, 2.1
		49, 22	23, 19	34, 16	35, 10	19, 9	23, 11	23, 11	8, 6	9, 7	7, 5	6, 4
	Sound	22, 90	16, 75	9, 64	22, 49	1, 23	9, 40	9, 41	1, 19	4, 22	1, 16	1, 12
		34, 2.4	37, 1.8	33, 2.5	28, 2.8	34, 2.0	34, 2.4	29, 2.7	34, 2.1	35, 2.2	31, 2.6	32, 2.3
		66, 31	38, 12	39, 30	39, 12	22, 8	23, 16	23, 11	16, 10	14, 9	12, 8	7, 9
	Plant	38, 128	24, 54	19, 112	19, 53	3, 24	5, 53	4, 36	2, 30	2, 24	2, 22	1, 26
		35, 2.0	36, 1.7	36, 2.0	34, 2.2	34, 1.7	37, 1.9	34, 2.1	35, 1.8	37, 1.8	35, 2.0	35, 1.9
NLOS	*NIST*	91, 112	60, 87	56, 82	55, 33	36, 71	38, 72	41, 25	27, 67	28, 64	29, 23	23, 24
	North	16, 595	20, 522	18, 418	20, 205	5, 258	7, 251	11, 160	5, 187	4, 170	4, 149	1, 140
		27, 4.6	25, 4.5	27, 4.6	23, 4.9	21, 4.7	27, 4.6	25, 4.8	24, 4.6	27, 4.5	26, 4.7	24, 4.6
	Child	107, 76	60, 60	68, 60	83, 52	44, 52	46, 42	53, 46	37, 35	31, 34	36, 37	29, 33
	Care	23, 372	10, 277	10, 282	10, 191	4, 238	5, 161	4, 174	4, 150	4, 127	3, 128	2, 127
		17, 6.4	18, 5.8	17, 6.4	13, 6.9	18, 5.6	17, 6.4	14, 7.0	19, 5.7	18, 6.3	16, 6.6	19, 5.8
		186, 190	113, 135	151, 157	142, 176	97, 112	88, 137	127, 228	72, 103	82, 119	102, 146	80, 124
	Sound	34, 783	21, 601	32, 612	32, 607	16, 515	22, 531	19, 527	7, 337	7, 348	7, 458	6, 408
		29, 5.2	28, 4.8	30, 5.1	30, 5.3	26, 4.8	30, 5.1	33, 5.2	28, 4.9	31, 5.0	31, 5.1	29, 4.9
		561, 578	473, 451	510, 520	557, 520	413, 444	397, 516	487, 511	339, 551	386, 512	430, 506	386, 602
	Plant	28, 2280	32, 1786	23, 2066	24, 2073	39, 1676	37, 2056	38, 1974	43, 2090	41, 2078	43, 1906	43, 2378
		38, 3.2	39, 2.8	38, 3.2	38, 3.3	37, 2.8	39, 3.2	39, 3.3	38, 2.9	40, 3.0	39, 3.2	39, 2.9

LEGEND
μ_e(cm), σ_e(cm)
$\min_e$(cm), $\max_e$(cm)
PL_0(dB), γ

TABLE III

STATISTICAL RESULTS FOR EXPERIMENTS.

ACKNOWLEDGEMENTS

The authors are indebted to Dr. Saeed S. Ghassemzadeh at AT&T Labs-Research for his guidance and advice in the design of the channel sounder.

REFERENCES

[1] A.F. Molisch, "Ultrawideband Propagation Channels-Theory, Measurement, and Modeling," *IEEE Trans. on Vehicular Technology*, Vol. 54, No. 5, Sept. 2005.

[2] D. Cassioli, M.Z. Win, and A.F. Molisch, "The Ultra-Wide Bandwidth Indoor Channel: From Statistical Model to Simulations," *IEEE Journal on Selected Areas in Communications*, vol. 20, no. 6, Aug. 2002.

[3] Z. Irahhauten, H. Nikookar, and G.J.M. Janssen, "An Overview of Ultra Wide Band Indoor Channel Measurements and Modeling," *IEEE Microwave and Wireless Components Letters*, vol. 14, No. 8, Aug. 2004.

[4] S.M. Yano, "Investigating the Ultra-Wideband Indoor Wireless Channel," *IEEE Conf. on Vehicular Technology, Spring*, pp. 1200-1204, May 2002.

[5] C. Prettie, D. Cheung, L. Rusch, and M. Ho, "Spatial Correlation OF UWB Signals in a Home Environment," *IEEE Conf. on Ultra Wideband Systems and Technologies*, pp. 65-69, May 2002.

[6] A. Durantini, W. Ciccognani, and D. Cassioli, "UWB Propagation Measurements by PN-Sequence Channel Sounding," *IEEE Conf. on Communications*, pp. 3414-3418, June 2004.

[7] A. Durantini and D. Cassioli, "A Multi-Wall Path Loss Model for Indoor UWB Propagation," *IEEE Conf. on Vehicular Technology, Spring*, pp. 30-34, May 2005.

[8] J. Kunisch and J. Pump, "Measurement Results and Modeling Aspects for UWB Radio Channel," *IEEE Conf. on Ultra Wideband Systems and Technologies*, pp. 19-24, May 2002.

[9] J. Keignart and N. Daniele, "Subnanosecond UWB Channel Sounding in Frequency and Temporal Domain," *IEEE Conf. on Ultra Wideband Systems and Technologies*, pp. 25-30, May 2002.

[10] S.S. Ghassemzadeh, L.J. Greenstein, T. Sveinsson, A. Kavcic, and V. Tarokh, "UWB Delay Profile Models for Residential and Commercial Indoor Environments," *IEEE Trans. on Vehicular Technology*, vol. 54, no. 4, July 2005.

[11] A.F. Molisch, K. Balakrishnan, D. Cassioli, C.-C. Chong, S. Emami, A. Fort, J. Karedal, J. Kunisch, H. Schantz, U. Schuster, and K. Siwiak, "A Comprehensive Model for Ultrawideband Propagation Channels," *IEEE Conf. on Global Communications*, pp. 3648-3653, March 2005.

[12] C. Gentile, "Sensor Location through Linear Programming with Triangle Inequality Constraints," *IEEE Conf. on Communications*, pp. 3192-3196, May 2005.

[13] B. Denis, J. Keignart, and N. Daniele, "Impact of NLOS Propagation upon Ranging Precision in UWB Systems," *IEEE Conf. on Ultra Wideband Systems and Technologies*, pp. 379-383, Nov. 2003.

[14] B. Denis and N. Daniele, "NLOS Ranging Error Mitigation in a Distributed Positioning Algorithm for Indoor UWB Ad-Hoc Networks," *IEEE Workshop on Wireless Ad-Hoc Networks*, pp. 356-360, June 2004.

[15] J.-Y. Lee and R.A. Scholtz, "Ranging in a Dense Multipath Environment Using and UWB Radio Link," *IEEE Journal on Selected Areas in Communications*, vol. 20, no. 9, Dec. 2002.

[16] D. Cassioli, A. Durantini, and W. Ciccognani, "The Role of Path Loss on the Selection of the Operating Band of UWB Systems," *IEEE Conf. on Personal, Indoor and Mobile Communications*, pp. 3414-3418, June 2004.

[17] H. Hashemi, "The Indoor Radio Propagation Channel," *Proceedings of the IEEE*, vol. 81, no. 7, pp. 943-968.

[18] A. Muqaibel, A. Safaai-Jazi, A. Bayram, A.M. Attiya, and S.M. Riad, "Ultrawideband through-the-wall propagation," *IEE Proc. on Microwaves, Antennas, and Propagation*, pp. 581-588, Dec. 2005.

[19] X. Li. and K. Pahlavan, "Super-Resolution TOA Estimation With Diversity for Indoor Geolocation," *IEEE Trans. on Wireless Communications*, vol. 3, no. 1, Jan. 2004.

[20] L. Hentila, V. Hovinen, and M. Hamalainen, "Sub-band Analysis in UWB Radio Channel Modeling," *Finnish Wireless Communications Workshop*, Aug. 2004.

[21] I. Guvenc and Z. Sahinoglu, "Threshold-Based TOA Estimation for Impulse Radio UWB Systems," *IEEE Conf. on Ultra Wideband Systems and Technologies*, pp. 420-425, Sept. 2005.

[22] I. Guvenc and Z. Sahinoglu, "Threshold Selection for UWB TOA Estimation Based on Kurtosis Analysis," *IEEE Communication Letters*, vol. 9, no. 12, pp. 1025-1027, Dec. 2005.